

NASA TECHNICAL NOTE



NASA TN D-8259 *c/*

NASA TN D-8259

LOAN COPY: RET
AFWL TECHNICAL
KIRTLAND AFB,



ABSOLUTE CALIBRATION OF THE RADSCAT SCATTEROMETER USING PRECISION SPHERES

*William L. Grantham, Lyle C. Schroeder,
and John L. Mitchell*

*Langley Research Center
Hampton, Va. 23665*



NATIONAL AERONAUTICS AND SPACE ADMINISTRATION • WASHINGTON, D. C. • DECEMBER 1976



0133985

1. Report No. NASA TN D-8259		2. Government Accession No.		3. Recipient's Catalog No.	
4. Title and Subtitle ABSOLUTE CALIBRATION OF THE RADSCAT SCATTEROMETER USING PRECISION SPHERES		5. Report Date December 1976		6. Performing Organization Code	
		8. Performing Organization Report No. L-10554		10. Work Unit No. 161-05-07-01	
7. Author(s) William L. Grantham, Lyle C. Schroeder, and John L. Mitchell		11. Contract or Grant No.		13. Type of Report and Period Covered Technical Note	
9. Performing Organization Name and Address NASA Langley Research Center Hampton, VA 23665		14. Sponsoring Agency Code			
12. Sponsoring Agency Name and Address National Aeronautics and Space Administration Washington, DC 20546					
15. Supplementary Notes John L. Mitchell: Vought Corporation, Hampton, Va.					
16. Abstract Tests using precision sphere targets suspended from balloons were conducted December 7 and 8, 1972, to calibrate the received-power—transmitted-power ratio of the RADSCAT scatterometer. Comparisons have been made of these measured results with theoretical return from spheres. These results show that the RADSCAT scatterometer measurements at 13.9 GHz should be corrected by -2.4 dB, and those at 9.3 GHz, by -4.3 dB. The techniques described herein should be generally applicable to calibration of scatterometers where measurement precision is of prime importance. Inferred from the magnitude of these RADSCAT corrections is the present state of technology in building precision scatterometers.					
17. Key Words (Suggested by Author(s)) Microwave scatterometer Sphere cross section Absolute calibration			18. Distribution Statement Unclassified - Unlimited Subject Category 48		
19. Security Classif. (of this report) Unclassified	20. Security Classif. (of this page) Unclassified	21. No. of Pages 43	22. Price* \$3.75		

ABSOLUTE CALIBRATION OF THE RADSCAT SCATTEROMETER

USING PRECISION SPHERES

William L. Grantham, Lyle C. Schroeder,
and John L. Mitchell*
Langley Research Center

SUMMARY

Tests using precision sphere targets suspended from balloons were conducted December 7 and 8, 1972, to calibrate the received-power—transmitted-power ratio of the RADSCAT scatterometer. Comparisons have been made of these measured results with theoretical return from spheres. These results show that the RADSCAT scatterometer measurements at 13.9 GHz should be corrected by -2.4 dB, and those at 9.3 GHz, by -4.3 dB.

The techniques described herein should be generally applicable to calibration of scatterometers where measurement precision is of prime importance. Inferred from the magnitude of these RADSCAT corrections is the present state of technology in building precision scatterometers.

INTRODUCTION

Microwave radar backscatter from the ocean has been shown to be sensitive to surface winds (for example, ref. 1). Aircraft measurements over the ocean are currently being made by the scientific community (refs. 2, 3, and 4) to characterize the correlation of radar scattering coefficient with surface winds. A combined radiometer-scatterometer (RADSCAT) is being used by NASA for this purpose.

In order for a scatterometer instrument to be a valuable tool for remote sensing, it must provide an accurate, absolute measurement of radar scattering coefficient. This is particularly true for RADSCAT, where ocean radar-scattering-coefficient measurements are to be used to infer surface wind velocity. It has been shown in reference 5, for example, that if wind speeds are 12 m/sec (23 knots), errors of less than 1 dB in radar cross section cause large errors in inferred wind speeds.

*Vought Corporation, Hampton, Va.

Historically, spheres have been used as a standard for back-scatter radar targets since they have no angular sensitivity and their cross sections can be calculated very accurately. For in-flight calibration of radar systems, however, even when precision spheres are used as calibration targets, an average accuracy of ± 2 dB is typical (ref. 6). Ground-based radar tests, if properly implemented, should yield less error. In this investigation both in-flight and ground-based evaluation tests were run on the RADSCAT system to determine its ability to measure radar cross section accurately.

In the ground-based tests, precision radar spheres of various sizes were used as radar targets to evaluate the absolute and relative accuracy of the instrument in the lower half of the instrument dynamic range. The sphere tests were performed with the RADSCAT bolted to a ground-based gimbaled mount, with the spheres suspended below free-flight weather balloons. Other sphere tests included fixed-range tests where the spheres were held aloft using a kytoon (a combination design of a kite and balloon). As will be discussed later, the kytoon test results were considered unsatisfactory for analysis.

In the in-flight tests, returns from triangular and square trihedral corner reflectors were measured during overflights. The results of the corner reflector tests are considered more qualitative in nature and are not discussed in this report.

SYMBOLS

Values are given in both SI and U.S. Customary Units. Measurements and calculations were made in U.S. Customary Units.

A	area, cm^2 (in^2)
a	attenuation, particularly of scatterometer channel, dB
a_{cl}	calibration loop attenuation, dB (GXR in ref. 7)
d	sphere diameter, cm (in.)
G	antenna gain, dB
L	distance between FPQ-6 radar and RADSCAT, m (ft)
P	power, dB
R	slant range, m (ft)
r	sphere radius, cm (in.)

t_o	time of sphere release
v	output voltage of scatterometer, V
β	equivalent pencil beam width (ref. 7), deg
ϵ_{rms}	root-mean-square variance or tolerance in $\left(\frac{P_r}{P_t G^2}\right)_{meas}$
ζ_o	root-mean-square surface roughness, cm (in.)
θ	incidence or off-boresight angle, deg
λ	wavelength, cm (in.)
σ	scattering cross section
σ^o	normalized scattering cross section or scattering coefficient
τ	integration time, sec
$\Delta\phi$	tracking-angle error, deg
ψ	angle between tracking radar and RADSCAT line of sight to sphere, deg

Subscripts:

bal	balloon
bs	boresight
cal	internal calibration level
max	maximum
meas	measured
min	minimum
r	received
reg	regulator
sea	experimental level from sea
sp	sphere
t	transmitted

tot total
tr tracking radar

SCATTEROMETER DESCRIPTION

The RADSCAT is a combined radiometer-scatterometer developed by the AAFE (advanced applications flight experiment) program to measure the scattering coefficient and brightness temperature of the ocean from an aircraft at 9.3 and 13.9 GHz. Since a detailed description of RADSCAT and its operation is given in reference 7 and since the radiometer subsystem is not pertinent to this investigation, only a brief description of the scatterometer is given herein.

A simplified block diagram of the scatterometer is given in figure 1. For scatterometer ocean measurements, pulses are transmitted from the antenna such that the area of the surface illuminated is defined by the antenna pattern with beam-filled conditions. RADSCAT uses a dual-polarized parabolic antenna with a full half-power beam width of about 1.5° . The transmitter is turned off during the pulse reception period to prevent transmitter leakage into the receiver. After turnoff, the scatterometer receiver is turned on by selectable range gates for periods which correspond to the slant-range pulse transit time. During this period, a sample of the backscattered pulse is processed. In the signal processor (fig. 1), four receiver channels (Scat channels) are used in parallel with staggered ranges of sensitivity to insure sensitivity over the large (approximately 60 dB) dynamic range of received signal from the ocean surface. In each channel, the signal is square-law detected and integrated for a selectable period ranging from 300 to 924 msec. The analog integrator outputs are then converted to digital outputs and recorded in a pulse-code-modulated (PCM) format on an analog magnetic tape. To minimize the importance of long-term drift, the instrument is automatically calibrated approximately every 2 min by switching a known sample of transmitter power into the receiver.

The transfer function of the normalized scattering coefficient σ^0 of RADSCAT has been derived in reference 7 and is

$$\sigma^0 = \frac{P_r}{P_t} \frac{(16\pi)^2 R^2 \cos \theta}{G^2 \lambda^2 \beta^2} = a \frac{v_{\text{sea}} \tau_{\text{cal}}}{v_{\text{cal}} \tau_{\text{sea}}} a_{\text{cl}} \frac{(16\pi)^2 R^2 \cos \theta}{G^2 \lambda^2 \beta^2} \quad (1)$$

APPARATUS AND TEST SITE

Ground-based RADSCAT calibration data were taken on two different days with precision radar spheres used as targets. The front-end assembly of the RADSCAT antenna was bolted to a gimbaled mount (fig. 2) which allowed variation in both azimuth and elevation. Control of the mount included a manual and a slave mode of operation. Control signals in the latter case came from a tracking radar system.

Two types of tests were conducted on the target spheres. In the first, spheres were sent aloft by using 1 kg (2.2 lbm) free-flight weather balloons (fig. 3) which ascended at a rate of about 300 m/min (985 ft/min). As the balloon and sphere ascended, a line regulator at the base of the weather balloon slowly deployed the sphere with 33.5 m (110 ft) of nylon line. The balloon and sphere were separated to avoid signal return from the weather balloon.

The effect of separating the balloon and the sphere at a range of 610 m (2000 ft) was to reduce the signal reflection of the balloon from -15 dB to -40 dB (relative to the 30.48-cm-diameter (12 in.) sphere). The 33.5-m (110 ft) separation distance kept the balloon out of the 3 dB beam radius until a range of approximately 2440 m (8000 ft) was reached. However, reflections from the balloon and regulator are considered in the error budget. (See appendix.)

By the time the balloon-sphere pair had drifted out to the minimum range of 580 m (1900 ft) required by RADSCAT range gating, the sphere elevation angle (approximately 45°) was high enough to avoid ground clutter. A potential source of interference in these tests was backscatter from the 0.076-cm-diameter (0.03 in.) nylon line between the balloon and the sphere (ch. 11 of ref. 8). By selecting the polarization of the transmitted RADSCAT signal to be perpendicular to the support line, this effect was reduced to essentially zero.

For the balloon-lofted sphere tests, two different spheres were used. Characteristics of the spheres are given in the following table:

	Small sphere	Large sphere
Diameter, cm (in.)	30.48 (12)	55.88 (22)
Material	Aluminum	Styrofoam with silver conducting paint
Weight, kg (oz)	0.908 (32)	0.794 (28)
Sphericity, cm (in.)	0.051 (0.020)	0.226 (0.089)
Surface finish, cm (in.)	0.0033 (0.0013)	0.0318 (0.0125)

The small spheres were precision targets, as can be seen from the preceding table. The large spheres were much lower in precision, but were used because larger aluminum spheres were difficult for the balloon to loft and were prohibitively costly to provide since the spheres were not recoverable. However, the sphericity and finish of the styrofoam spheres were small relative to wavelength (2 to 3 cm (0.8 to 1.2 in.)) at 13.9 GHz and 9.3 GHz.

In the second type of test, the spheres were suspended below a 9.15-m-long (30 ft) helium-filled kytoon (fig. 4) and held by tethering at a range from the RADSCAT of approximately 2300 m (7500 ft) (fig. 5). Larger spheres could be held in range for longer periods of time with a kytoon than with a free-flight balloon. Also, the same spheres could be used repeatedly with the kytoon, whereas the balloon and sphere were not recoverable after the free-flight tests. Two disadvantages limited the results obtained in the kytoon-sphere tests. First, three large 2224-N test (500 lbf) nylon tether lines, which were required to stabilize the kytoon, produced cross section measurement errors. Second, the maximum elevation angle was limited to about 5.5° as a result of the weight of the spheres and the tether lines, which meant there was some ground clutter reducing the accuracy of the measurements. The errors caused by the presence and motion of the tether lines were felt to be minor, but the inaccuracies resulting from the low elevation angle were felt to be great; for this reason the kytoon-sphere data are not being analyzed.

Aircraft-based in-flight RADSCAT calibration tests were conducted over the runway of the NASA Wallops Flight Center and at the U.S. Army Radar Geometric Fidelity Array at Willcox, Arizona. In these tests, flights over corner reflectors were used to produce a return in the upper half of the scatterometer dynamic range; thus, the sphere and the corner reflector tests together covered the complete scatterometer dynamic range. The corner reflector tests were completely independent of the ground-based tests and will not be discussed further because they were qualitative in nature.

SPHERE TRACKING METHOD

The balloon-sphere combination was released near the gimbal-mounted RADSCAT instrument on Wallops Island, as shown in figure 5, and was tracked with the FPQ-6 radar located on the mainland. The FPS-16 radar, located on Wallops Island, was used as an alternate tracker. During each test the RADSCAT was positioned at a surveyor's mark so that translation of coordinates from the FPQ-6 to the RADSCAT could be accurately made and thus allow proper parallax corrections. Real-time signals for the RADSCAT

mount drive were provided by the FPQ-6 radar to allow a hands-off tracking mode if desired.

In order to permit visual tracking of the sphere from the RADSCAT test site and to provide a record of tracking history, a boresighted television camera, monitor, and video recorder were installed (fig. 2). The boresighted camera was calibrated by scanning the gimbal mount vertically and horizontally across an optical target. The boresight offset angle from the RADSCAT antenna beam was later determined by measuring the angle recorded by the boresighted camera during peak RADSCAT return (compensated for range) from a free-flight sphere. Estimated errors for the sphere test are given in the appendix.

SPHERE TEST RESULTS

Experimental data with which to calibrate the absolute level of the RADSCAT scatterometer return were obtained on December 7 and 8, 1972, at Wallops Flight Center. The calibration should be valid for RADSCAT from September 1, 1972, to December 1, 1973, since no changes were made in the system during this period. Balloons and kytoons were successfully launched and satisfactory tracking data were obtained, although for reasons previously discussed, only the balloon-sphere data were analyzed. Test data were obtained by using two different size spheres at both 13.9 and 9.3 GHz. Analog tape recordings of the PCM experiment data were obtained for computer processing. However, preliminary analysis using the strip charts was done to provide some insight into the validity of the results.

COMPARISON OF THEORY WITH STRIP CHART RESULTS

Scatterometer return from the small sphere measured by the RADSCAT is shown in the pen record of figure 6 for 13.9 GHz. The level of the channels labeled Scat 4 and Scat 3 is proportional to the power return; a corresponding level for Scat 3 is about 19 dB higher than that for Scat 4. Increasing time (from right to left) on this chart is roughly equivalent to increasing sphere range.

First returns show that the signal abruptly rises to saturation for Scat 4 and is at a low level for Scat 3. This rise corresponds to the lower threshold of the RADSCAT 610-m (2000 ft) range gate. As slant range (time) increases, the scatterometer return decreases and falls into the range of Scat 4. An abrupt change in level occurs when the RADSCAT mode was switched, as indicated by the label "change mode integration time"; this is because the

integration time of the output decreased by $\frac{0.580}{0.924}$ at that time.

The Scat 4 return decreases with range from this time on except for the sharp rise that occurs when the RADSCAT mode was switched back to the initial mode integration time. Small periodic fluctuations noted on the trace are attributed to errors in the sphere tracking. Similar results are noted in the subsequent pen recordings in figures 7 to 9. Also, although the resolution on the strip charts is not great, the signal level at both frequencies appears higher from the large sphere than from the small sphere.

Calculations were made to compare the expected level of signal return from spheres with the dynamic range of the RADSCAT instrument. These calculations were made initially to aid in selecting spheres for the tests; however, they also provided predictions of results. These calculations were made in terms of the received power P_r normalized by the transmitter power P_t . The dynamic

range and the calibration level of each of the four channels of the RADSCAT scatterometer processor were determined by using the transfer function (see eq. (1))

$$\frac{P_r}{P_t} = a \frac{v_{\text{sea}} \tau_{\text{cal}}}{v_{\text{cal}} \tau_{\text{sea}}} a_{\text{cl}} \quad (2)$$

and the instrument characteristics of RADSCAT from reference 7. The signal return from the sphere was obtained by using the following theoretical expression derived from definitions in reference 8:

$$\frac{P_r}{P_t} = \frac{G_{\lambda}^2 2_{\sigma}}{(4\pi)^3 R^4} = \frac{G_d^2 2_{\lambda}^2}{(16\pi)^2 R^4} \quad (3)$$

where d is the sphere diameter and σ is approximately equal to $\pi d^2/4$.

Figure 10 is a composite showing the ranges of the calibrated boresight signal level P_r/P_t at 13.9 GHz for the four Scat channels of RADSCAT on the left-hand side and the curves of theoretical P_r/P_t to be expected for appropriately sized spheres as a function of range on the right-hand side. Shown also for comparison are the values of P_r/P_t expected from corner reflectors used

in other calibration tests as a function of range. Figure 11 is the corresponding plot for 9.3 GHz. In general, these plots indicate the following responses of the RADSCAT to the spheres:

(1) At a range of approximately 610 m (2000 ft), where the first returns uninhibited by the range gate are seen from the spheres, the signals from both spheres are in the lower part of Scat 3, with the larger sphere producing more return. These results are in agreement with strip chart observations.

(2) The signals from both spheres decrease at the rate of 12 dB for each doubling of range. Hence, the signal drops into Scat 4 before a range of about 915 m (3000 ft) is reached. This also agrees with strip chart results.

A preliminary comparison of measured returns on the strip charts in figures 6 to 9 with the responses shown in figures 10 and 11 indicates good general agreement, and thus, further analysis is warranted.

SPHERE DATA ANALYSIS

Data required for instrument evaluation came from three sources (fig. 12): from RADSCAT, which gives a measure of returned power as a function of time, from the FPQ-6 or FPS-16 tracking radars, which give a measure of range between RADSCAT and the sphere, and from the video tape made with the boresighted camera, which gives a history of the tracking error. Signal level compensations due to tracking errors were computed by using the measured antenna pattern shape near the beam axis (fig. 13).

For interpretation of results of these tests, theoretical values of $P_r/P_t G^2$ are computed from equation (3) for the conditions of these tests as follows:

$$\frac{P_r}{P_t G^2} = \frac{\lambda^2 \sigma}{(4\pi)^3 R^4} \quad (4)$$

Theoretical values were obtained by inserting into this equation the theoretical expression for radar cross section of a sphere $\sigma = \pi r^2$. (A Mie series approximation yields higher accuracy, but the resulting error is of small order; see the appendix.) The antenna gain G

is kept on the left side of the equation so that only sphere radius and range influence the theoretical values of $P_r/P_t G^2$.

Likewise, experimental values of $P_r/P_t G^2$ have been determined from the RADSCAT-sphere data as a function of range, with corrections made to allow for small off-boresight tracking errors. The experimental values of $P_r/P_t G^2$ for the sphere were calculated by inserting sphere-measured cross sections into equation (4). The σ_{sphere} data used are obtained from the σ_{Sea}^0 output of the RADSCAT instrument conversion program (see ref. 9) by using

$$\sigma_{\text{sp, meas}} = \frac{\pi(R\beta)^2}{4} \sigma_{\text{Sea}}^0 \quad (5)$$

The factor $\pi(R\beta)^2/4$ is required to denormalize the values of σ_{Sea}^0 that were calculated for the beam-filled case, since the sphere is not large enough to fill the beam. Thus,

$$\left(\frac{P_r}{P_t G^2} \right)_{\text{sp, meas}} = \frac{\lambda^2(\beta)^2}{(16\pi)^2 R^2} \sigma_{\text{Sea}}^0 \quad (6)$$

A comparison of theoretical and experimental $P_r/P_t G^2$ values is shown in figures 14, 15, 16, and 17. Included are the tests at 9.3 and 13.9 GHz for both sphere sizes. A constant offset between the measured and theory curves can be interpreted as a lumped bias in the scatterometer constants used to obtain the measured value. The offset "error" or bias, determined by the following expression, is given for each test in table I:

$$\text{Bias error} = \left(\frac{P_r}{P_t G^2} \right)_{\text{sp, theory}} - \left(\frac{P_r}{P_t G^2} \right)_{\text{sp, meas}} \quad (7)$$

The test results at 13.9 GHz from both spheres show a difference of from 1.9 to 2.4 dB above theoretical values of $P_r/P_t G^2$

(figs. 14 and 15). Since the experimental curve is nearly parallel to the theoretical curve, it shows a fourth-power dependence on range as it should. The exponents of range are -3.92424 and -3.95046 for the small and large spheres, respectively. If the RADSCAT detector diodes (in Scat channels 3 and 4) were not square-law detectors as assumed, it would show up here in the slope. The data points indicated in figures 14 and 15 were obtained in both Scat channels 3 and 4. The tolerances listed in table I are calculated and discussed in the appendix.

Test results at 9.3 GHz (figs. 16 and 17) show the data to be biased from 2.0 to 4.3 dB above theoretical values. The reason for the 2.3 dB difference in results is unknown, but the data for the small sphere are considered more accurate. The slope of the data also indicates, as expected, a fourth-power dependence on range as did the results at 13.9 GHz. Actual exponents of range are -4.44908 and -4.06934 for the small and large spheres, respectively. Limited data are shown for the large sphere as a result of delayed acquisition of the sphere by the tracking radar (data only in Scat 4).

In applying these results to RADSCAT, it should be noted that the small sphere was a precision metal sphere with known reflectivity, whereas the large sphere was a styrofoam sphere much less precise in dimensions and sprayed with a reflective paint. Thus, quantitative results from just the small sphere should be applied to the RADSCAT instrument, and those of the large sphere should be used only for comparison purposes.

CONCLUDING REMARKS

Tests using precision sphere targets suspended from balloons have been conducted to calibrate the received-power—transmitted-power ratio of the RADSCAT scatterometer. The techniques described herein should be generally applicable to calibration of scatterometers where measurement precision is of prime importance. Comparisons have been made of these measured results with theoretical return from spheres. These results show that the RADSCAT scatterometer measurements at 13.9 GHz should be corrected by -2.4 dB, and those at 9.3 GHz, by -4.3 dB. Inferred from the magnitude of these RADSCAT corrections is the present state of technology in building precision scatterometers and the impact of small component errors that accumulate into significant system errors.

Langley Research Center
National Aeronautics and Space Administration
Hampton, VA 23665
September 1, 1976

APPENDIX

ERROR BUDGET FOR SPHERE TESTS

The purpose of this appendix is to estimate the uncertainties in σ_{meas}^0 due to the errors which were not or could not be eliminated during the sphere calibrations of the RADSCAT radar. Errors considered are balloon and support line interference, ground clutter, sphere dimensional tolerances, off-boresight correction tolerance, sphere surface roughness, and tracking radar range and angle errors. A discussion of these error sources and the methods and assumptions involved in evaluating the errors are presented. These errors are summed to provide an estimate of tolerance on the sphere calibrations. While these errors may not be all inclusive, the error estimate should be of the right order of magnitude.

Error Due to Balloon and Regulator Interference

If the balloon and regulator are within the pencil beam of the radar, a return will be received which cannot be distinguished from that of the sphere. This error was minimized by separating the balloon and regulator from the sphere by 33.5 m (110 ft) of nylon string, which for short range moves the balloon and regulator away from the high gain part of the radar antenna pattern. At higher ranges, the balloon is much closer to peak gain, so an evaluation was made. The following information was used to evaluate the error:

$$\sigma_{\text{reg}} = A_{\text{reg,max}} = \left(\frac{d}{2}\right)^2 \pi = 14.51\pi \text{ cm}^2 (2.25\pi \text{ in}^2) \text{ for a } 7.62\text{-cm-diameter (3 in.) regulator.}$$

$$\sigma_{\text{bal}} = -15 \text{ dB relative to } \sigma \text{ of small sphere at boresight.}$$

This was measured during the current investigation.

$$\sigma_{\text{sp}} \approx \pi r^2 = 232.25\pi \text{ cm}^2 (36\pi \text{ in}^2) \text{ for small sphere and } 780\pi \text{ cm}^2 (121\pi \text{ in}^2) \text{ for large sphere.}$$

Hence, at boresight, the following relationships hold:

APPENDIX

	Small sphere	Large sphere
$\frac{\sigma_{reg}}{\sigma_{sp}}$	0.0625	0.0186
$\frac{\sigma_{bal}}{\sigma_{sp}}$	0.0316	0.00942
$\frac{\sigma_{reg} + \sigma_{bal}}{\sigma_{sp}}$	0.0941	0.0280

To calculate the error due to the balloon and regulators, it was assumed that the antenna was boresighted at the sphere and that the off-boresight contributions were being obtained from the balloon and regulator. Thus, the error was calculated by using

$$\sigma_{error} = \frac{\sigma_{tot}}{\sigma_{sp}} = \frac{\sigma_{sp} \Big|_{\theta_{bs}=0} + (\sigma_{bal} + \sigma_{reg}) \Big|_{\theta_{bs}=\frac{33.5}{R}}}{\sigma_{sp} \Big|_{\theta_{bs}=0}}$$

where R is in meters. But,

$$(\sigma_{bal} + \sigma_{reg}) \Big|_{\theta_{bs}=\frac{33.5}{R}} = (\sigma_{bal} + \sigma_{reg}) \left(\frac{G \Big|_{\theta_{bs}=0}}{G \Big|_{\theta_{bs}=\frac{33.5}{R}}} \right)$$

The errors were thus evaluated by obtaining the gain ratio from the patterns for that antenna. (Patterns used were those of January 1972.) E-plane values were used and in all cases gave errors approximately the same as H-plane values. The error was evaluated for three ranges: 610 m (2000 ft) (minimum range gate), 914 m (3000 ft) (mean), and 1829 m (6000 ft) (maximum range for system sensitivity). The values obtained are given in table II.

APPENDIX

Ground Clutter Error

To calculate the error due to ground clutter, the ground return at grazing incidence between the limits of the range gates, 610 m to 1829 m (2000 ft to 6000 ft), was calculated. The geometry is shown in figure 18. From reference 8 the relationship is

$$\begin{aligned} \left(\frac{P_r}{P_t}\right)_{\text{clutter}} &= \frac{G^2 \lambda^2 \sigma^0 A_T}{(4\pi)^3 R^4} = \frac{K}{(4\pi)^3} \int_{R_1}^{R_2} \int_{-\pi/2}^{\pi/2} \frac{R \, dR \, d\theta}{R^4} \\ &= \frac{K\pi}{(4\pi)^3} \int_{R_1}^{R_2} \frac{dR}{R^3} = \frac{K\pi}{2(4\pi)^3} \left(\frac{1}{R_1^2} - \frac{1}{R_2^2} \right) \end{aligned}$$

where $K = G^2 \lambda^2 \sigma^0$ and A_T is the radar target area. When converted to decibels, the preceding expression is

$$\left(\frac{P_r}{P_t}\right)_{\text{clutter}} = K - 87.23 = G^2 + \lambda^2 + \sigma^0 - 87.23$$

For RADSCAT, the following constants were used:

	13.9 GHz	9.3 GHz
λ^2	-33.32 dB	-29.83 dB
G^2	-14.7 dB	-5.5 dB
σ^0	-35 dB	-35 dB

The X-band σ^0 at grazing incidence was obtained from reference 3. Thus, for 13.9 GHz,

$$\left(\frac{P_r}{P_t}\right)_{\text{clutter}} = \underbrace{G^2}_{-14.7} - \underbrace{\lambda^2}_{33.32} - \underbrace{\sigma^0}_{35} - 87.23 = -170.2 \text{ dB}$$

APPENDIX

and for 9.3 GHz,

$$\left(\frac{P_r}{P_t}\right)_{\text{clutter}} = \underbrace{G^2}_{-5.5} - \underbrace{\lambda^2}_{29.83} - \underbrace{\sigma^0}_{35} - 87.23 = -157.6 \text{ dB}$$

The ground clutter error for 9.3 GHz and 13.9 GHz at ranges of 610 m (2000 ft), 914 m (3000 ft), and 1829 m (6000 ft) for the two spheres is obtained from the following:

$$\sigma_{\text{error}} = \frac{\left(\frac{P_r}{P_t}\right)_{\text{sp}} + \left(\frac{P_r}{P_t}\right)_{\text{clutter}}}{\left(\frac{P_r}{P_t}\right)_{\text{sp}}}$$

Results are tabulated in table II.

Calculation of Error Due to Off-Boresight Angle Uncertainty

An error exists as a result of imprecise knowledge of the off-boresight angle. The calculated precision with which the off-boresight angle can be determined from the video boresight monitor is $\pm 0.07^\circ$. Hence the off-boresight angle correction has a potential error resulting from this tolerance in precision.

To evaluate these errors, a second-order regression fit to the pattern data of figure 13 was made, and the following relationships were obtained:

at 9.3 GHz

$$\text{E-plane: } G = -(0.02959 + 2.25936\theta^2)$$

$$\text{H-plane: } G = -(-0.05388 + 2.16336\theta^2)$$

at 13.9 GHz

$$\text{E-plane: } G = -(-0.17650 + 6.21196\theta^2)$$

$$\text{H-plane: } G = -(-0.02468 + 4.2507\theta^2)$$

where θ is the off-boresight angle. These relationships were used to evaluate the differential gain between the nominal boresight angle and the nominal value $\pm 0.07^\circ$. A graphical interpolation of

APPENDIX

the actual data was used at points where the regression slope appeared in error (mainly at 0° off-boresight angle). The error in σ^0 is twice the gain error obtained, if the gain error is expressed in dB.

This error has been calculated at off-boresight angles of 0° and 0.5° , the maximum permissible range of values. This error was also calculated at angles of 0.25° and 0.40° , since 99 per-cent of the sphere data of this analysis were obtained between these values. (This span of off-boresight angles indicates that electrical and optical boresights were not aligned.) Worst-case estimates occur in the E-plane, but the H-plane estimates are also included in the following table. An abbreviated set of estimates is given in table II.

Off-boresight angle, deg	Boresight angle precision error, dB, at -			
	9.3 GHz for -		13.9 GHz for -	
	E-plane	H-plane	E-plane	H-plane
0 ± 0.07	*0 -.03	*0 -.016	*0 -.073	*0 -.054
0.25 ± 0.07	.136 -.18	.13 -.173	*.26 -.28	.256 -.339
0.40 ± 0.07	.231 -.275	.221 -.264	.635 -.757	.434 -.518
0.50 ± 0.07	.293 -.339	.282 -.324	.808 -.932	.533 -.637

*Indicates graphical determination.

Calculation of Error Due to Surface Roughness of Spheres

The normalized variance in cross section $D\{\sigma\}$ due to surface roughness can be estimated from equation (8) in reference 10 as

$$D\{\sigma\} \approx 32\pi^2(\zeta_0/\lambda)^2$$

where ζ_0 is the rms roughness (0.003302 cm (0.0013 in.) for the small sphere and 0.03175 cm (0.0125 in.) for the large sphere) and λ is the radar wavelength. Although this estimate is for circular polarization, it is useful to find the magnitude of the error

APPENDIX

for this case. The error in cross section is calculated by using the following equation of reference 10:

$$\text{Roughness error [dB]} = 4.35(D\{\sigma\})^{1/2}$$

The errors obtained are given in table II.

Calculation of Error Due to Dimensional Tolerance of Spheres

An error in cross section occurs due to variation δ of the dimensional (i.e., the diameter) tolerance of the spheres. This error has been estimated by calculating the cross section σ for a sphere with diameter $d \pm \delta$. Mie theory was used with enough terms retained to obtain accuracies to 0.01 percent. Sphere diameter variance values used were ± 0.381 cm (± 0.015 in.) for the small sphere and ± 0.1143 cm (± 0.045 in.) for the large sphere. These values of δ are equal or greater than the measured values given in the main text. Resulting errors due to dimensional tolerance were evaluated and are given in table II.

Error Due to Range and Angle Errors of the Tracking Radar

From Nathan Novak of Wallops Flight Center, the following error estimates were obtained for skin tracking a sphere with the FPQ-6 radar:

Range error (rms) $\Delta R_{tr} = \pm 1$ to 5 m (3.3 to 16.4 ft) (more data are needed)

Tracking-angle error (rms) $\Delta \phi_{tr} = \pm 0.0001$ radian

These errors would result in a variance in the scattering cross section due to imprecise knowledge of slant range R in equation (4). This variance can be computed as

$$\sigma_{\text{error}} = \left(\frac{R + \Delta R}{R} \right)^4$$

where ΔR is the range error.

The geometry of the situation is shown in figure 19. The component of ΔR along the RADSCAT line of sight is

$$\Delta R = \Delta R_{tr} \cos \psi$$

APPENDIX

The angle ψ is determined by the law of sines as

$$\psi = \frac{L \sin 130}{R_{tr}}$$

where L , the distance between the FPQ-6 radar and RADSCAT, is scaled to be 4635 m (15 206 ft), and 130° is the angle formed by the FPQ-6—RADSCAT line of sight and the RADSCAT-sphere line of sight. (The assumption is that the balloon drifts out perpendicular to the shore.) Since

$$R_{tr} = \sqrt{R^2 + 2LR \sin 130 + L^2}$$

from the law of cosines, the error can be evaluated.

The component of error due to the radar tracking-angle error $\Delta\phi_{tr}$ is evaluated by finding the resulting component of error in RADSCAT slant range. This range error is

$$\Delta R = R_{tr} \Delta\phi_{tr} \cos(90 - \psi)$$

Results of the calculations for range error and tracking-angle error due to the tracking radar are presented separately in the following table and as summed values in table II:

RADSCAT slant range, m (ft)	R_{tr} , m (ft)	ψ , deg	Component due to range error		Component due to angle error	
			ΔR , m (ft) (a)	σ_{error} , dB	ΔR , m (ft) (b)	σ_{error} , dB
610 (2000)	5049 (16 565)	44.68	3.56 (11.68)	0.102	0.35 (1.15)	0.010
914 (3000)	5269 (17 287)	42.36	3.69 (12.11)	.070	.36 (1.18)	.0066
1829 (6000)	5977 (19 610)	36.44	4.02 (13.19)	.038	.36 (1.18)	.0033

^a ΔR_{tr} was assumed to be ± 5 m (16.4 ft).

^b $\Delta\phi_{tr}$ was assumed to be ± 0.0001 radian.

Error Summation

Errors were summed in two ways. First, errors were summed linearly according to whether they increase or decrease σ^0 to obtain an outer limit of tolerance for the σ^0 measurements (and hence the tolerances on the sphere correction factor). Referring

APPENDIX

to equations (6) and (7), it is seen that errors which increase σ_{tot}^0 result in a positive bias tolerance, and vice versa. This summing is shown in table III.

Second, errors were summed in an rms fashion to obtain an estimate of the most probable one standard deviation error. The method used to handle errors which were slightly nonsymmetrical was to record the nonzero mean and then calculate the variance about the point of symmetry. For errors which were all positive (or negative), the nonzero mean was recorded and the value of variance was calculated using

$$\text{Variance} = \frac{1}{2}(\text{error})^2$$

This technique was suggested by L. Wilson of the Vought Corporation. Results of the rms summing are given in table IV. The rms variance ϵ in dB is calculated using

$$\epsilon = 10 \log_{10} \left(1 + \sqrt{\sum \text{variance}} \right)$$

Discussion of Error Budget Results


Some comments can be made regarding the error values obtained and given in table II:

(1) The balloon and regulator interference error is insignificant except at maximum range and, hence, is probably unimportant for these tests.

(2) The ground clutter error is clearly orders of magnitude below the other errors.

(3) The error due to boresight angle precision is significant, and precision must be used in every phase of the boresight correction procedure. This error increases as antenna beam width gets smaller. In this case, alinement of optical with electrical boresight would have reduced the worst case tolerances on error bias by an estimated 0.15 to 0.25 dB at 9.3 GHz and from 0.25 to 0.65 dB at 13.9 GHz.

(4) Dimensional tolerance in the sphere caused relatively unimportant errors.



APPENDIX

(5) Surface roughness of the spheres is an important consideration; in fact, it is the most important error source for the large sphere.

(6) The errors due to support line and net, which were only estimated, are probably less than indicated.

(7) More data are required on the accuracy of range tracking of spheres, even though the error does not appear to be large.

REFERENCES

1. Apel, John R.: A Hard Look at Oceans From Space. AIAA Paper No. 73-11, Jan. 1973.
2. Jones, W. Linwood; Grantham, William L.; Schroeder, Lyle C.; and Mitchell, John L.: Microwave Scatterometer Measurements of Ocean Wind Vector. Paper presented at the 1974 UNSC/URSI - IEEE Meeting (Boulder, Colorado), Oct. 14-17, 1974.
3. Daley, John: An Empirical Sea Clutter Model. NRL Mem. Rep. 2668, U.S. Navy, Oct. 1973.
4. Krishen, K.: Correlation of Radar Backscattering Cross Sections With Ocean Wave Height and Wind Velocity. J. Geophys. Res., vol. 76, no. 27, Sept. 20, 1971, pp. 6528-6539.
5. Grantham, W. L.; Bracalente, E. M.; Jones, W. L.; Schrader, J. H.; Schroeder, L. C.; and Mitchell, J. L.: An Operational Satellite Scatterometer for Wind Vector Measurements Over the Ocean. NASA TM X-72672, 1975.
6. Guinard, Norman W.; and Daley, John C.: An Experimental Study of a Sea Clutter Model. Proc. IEEE, vol. 58, no. 4, Apr. 1970, pp. 543-550.
7. Schroeder, Lyle C.; Jones, W. L., Jr.; and Mitchell, John L.: Laboratory Calibration of AAFE Radiometer/Scatterometer (RADSCAT). NASA TM X-73900, 1976.
8. Ruck, George T.; Barrick, Donald E.; Stuart, William D.; and Krichbaum, Clarence K.: Radar Cross Section Handbook. Volume 2. Plenum Press, Inc., 1970.
9. Claassen, John P.: AAFE RADSCAT Data Reduction Programs User's Guide. NASA CR-144992, 1973.
10. Burrows, M. L.: Surface Tolerance of a Radar Calibration Sphere. IEEE Trans. Antennas & Propag., vol. AP-16, no. 6, Nov. 1968, pp. 718-724.

TABLE I.- BIAS ERRORS AND TOLERANCES IN MEASURED VALUES OF $P_r/P_t G^2$

[Error calculation method is shown in figs. 14 to 17]

Frequency, GHz	Sphere	Bias error, dB	Worst case tolerances, dB, at -		rms tolerances, dB, at -			
			$\theta_{bs,min} = 0.25^\circ$	$\theta_{bs,max} = 0.40^\circ$	$\theta_{bs,min} = 0.25^\circ$		$\theta_{bs,max} = 0.40^\circ$	
					ϵ_{rms}	Bias	ϵ_{rms}	Bias
13.9	Small	2.4	0.67 -.49	1.04 -.96	0.33	0.09	0.72	0.04
13.9	Large	1.9	1.68 -1.50	2.05 -1.98	1.04	.09	1.20	.04
9.3	Small	4.3	.51 -.35	.60 -.44	.24	.08	.31	.08
9.3	Large	2.0	1.18 -1.02	1.27 -1.12	.73	.08	.75	.07

TABLE II.- ESTIMATED ERRORS FOR RADSCAT TESTS

Error source	Error, dB, at -			
	9.3 GHz for -		13.9 GHz for -	
	Small sphere	Large sphere	Small sphere	Large sphere
Balloon and regulator interference at range of -				
610 m (2000 ft)	1×10^{-5}	3.1×10^{-6}	5.8×10^{-6}	1.8×10^{-6}
914 m (3000 ft)	1×10^{-3}	3.1×10^{-4}	8.9×10^{-4}	2.6×10^{-5}
1829 m (6000 ft)	.101	.03	.016	4.8×10^{-3}
Ground clutter at range of -				
610 m (2000 ft)	2.3×10^{-5}	6.9×10^{-6}	1.6×10^{-6}	4.8×10^{-7}
914 m (3000 ft)	1.0×10^{-4}	3.3×10^{-5}	8.7×10^{-6}	2.6×10^{-6}
1829 m (6000 ft)	1.8×10^{-3}	5.5×10^{-4}	1.3×10^{-4}	4.3×10^{-5}
Correction for off-boresight angle of -				
$0.25^\circ \pm 0.07^\circ$.14	.14	.26	.26
	-.18	-.18	-.28	-.28
$0.40^\circ \pm 0.07^\circ$.231	.231	.635	.635
	-.275	-.275	-.757	-.757
Surface roughness of spheres	.079	.761	.118	1.138
Dimensional tolerance of spheres	.0154 -.0130	-.0057 -.0022	.012 -.011	-.0070 .0042
Support line and net (ref. 8)	<.2	<.2	<.2	<.2
Tracking radar range and angle error (sum) at range of -				
610 m (2000 ft)	$\pm .112$	$\pm .112$	$\pm .112$	$\pm .112$
914 m (3000 ft)	$\pm .077$	$\pm .077$	$\pm .077$	$\pm .077$
1829 m (6000 ft)	$\pm .041$	$\pm .041$	$\pm .041$	$\pm .041$

TABLE III.- EFFECT OF ERRORS ON σ_{tot}^0

Error source	Error in σ_{tot}^0 , dB, at -							
	9.3 GHz for -				13.9 GHz for -			
	Small sphere		Large sphere		Small sphere		Large sphere	
	Increase	Decrease	Increase	Decrease	Increase	Decrease	Increase	Decrease
Balloon and regulator	1×10^{-3}	0	3.1×10^{-4}	0	8.9×10^{-4}	0	2.6×10^{-5}	0
Ground clutter	1×10^{-4}	0	3.3×10^{-5}	0	8.7×10^{-6}	0	2.6×10^{-6}	0
Correction for off-boresight angle of -								
0.25°	.14	.18	.14	.18	.26	.28	.26	.28
0.40°	.231	.275	.231	.275	.635	.757	.635	.757
Surface roughness	.079	.079	.761	.761	.118	.118	1.138	1.138
Dimensional tolerance	.0154	.013	0	.0057	.012	.011	.0042	.007
Net and lines	.2	0	.2	0	.2	0	.2	0
Tracking radar range and angle error	.077	.077	.077	.077	.077	.077	.077	.077
Total at $\theta_{\text{bs}} = 0.25^\circ$	0.513	0.349	1.178	1.024	0.668	0.486	1.679	1.502
Total at $\theta_{\text{bs}} = 0.40^\circ$.604	.444	1.269	1.119	1.043	.963	2.054	1.979

TABLE IV.- rms SUMMING

Error source	rms error at -							
	9.3 GHz for -				13.9 GHz for -			
	Small sphere		Large sphere		Small sphere		Large sphere	
	Nonzero mean, dB	Variance (a)	Nonzero mean, dB	Variance (a)	Nonzero mean, dB	Variance (a)	Nonzero mean, dB	Variance (a)
Balloon and regulator	5×10^{-4}	2.66×10^{-8}	1.55×10^{-4}	2.56×10^{-9}	4.45×10^{-4}	2.10×10^{-11}	1.3×10^{-5}	1.79×10^{-11}
Ground clutter	5×10^{-5}	2.65×10^{-10}	1.65×10^{-5}	2.89×10^{-11}	4.35×10^{-6}	2.01×10^{-12}	1.3×10^{-6}	1.79×10^{-13}
Correction for off-boresight angle of -								
0.25°	-2×10^{-2}	1.41×10^{-3}	-2×10^{-2}	1.41×10^{-3}	-1×10^{-2}	4.10×10^{-3}	-1×10^{-2}	4.10×10^{-3}
0.40°	-2.5×10^{-2}	3.65×10^{-3}	-2.5×10^{-2}	3.65×10^{-3}	-6×10^{-2}	3.06×10^{-2}	-6×10^{-2}	3.06×10^{-2}
Surface roughness	0	3.31×10^{-4}	0	3.06×10^{-2}	0	7.40×10^{-4}	0	6.84×10^{-2}
Dimensional tolerance	1.2×10^{-2}	1.07×10^{-5}	-2.8×10^{-2}	8.62×10^{-7}	0	7.16×10^{-6}	-1.4×10^{-3}	1.66×10^{-6}
Net and lines	1×10^{-1}	1.11×10^{-3}	1×10^{-1}	1.11×10^{-3}	1×10^{-1}	1.11×10^{-3}	1×10^{-1}	1.11×10^{-3}
Tracking radar range and angle error	0	3.20×10^{-4}	0	3.20×10^{-4}	0	3.20×10^{-4}	0	3.20×10^{-4}
Σ variance at $\theta_{bs} = 0.25^\circ$		3.18×10^{-3}		3.35×10^{-2}		6.28×10^{-3}		7.40×10^{-2}
$\sqrt{\Sigma}$ variance at $\theta_{bs} = 0.25^\circ$		5.64×10^{-2}		1.83×10^{-1}		7.92×10^{-2}		2.72×10^{-1}
Total nonzero mean at $\theta_{bs} = 0.25^\circ$	0.082		0.077		0.090		0.088	
rms variance, dB, at $\theta_{bs} = 0.25^\circ$.238		.729		.331		1.045
Σ variance at $\theta_{bs} = 0.40^\circ$		5.42×10^{-3}		3.57×10^{-2}		3.27×10^{-2}		1.00×10^{-1}
$\sqrt{\Sigma}$ variance at $\theta_{bs} = 0.40^\circ$		7.36×10^{-2}		1.89×10^{-1}		1.81×10^{-1}		3.17×10^{-1}
Total nonzero mean at $\theta_{bs} = 0.40^\circ$.077		.072		.040		.039	
rms variance, dB, at $\theta_{bs} = 0.40^\circ$.309		.751		.722		1.195

^aVariance values are in dimensionless ratio form and are calculated for one-sided errors by using $(\text{error})^2/2$, where the error is from table III.

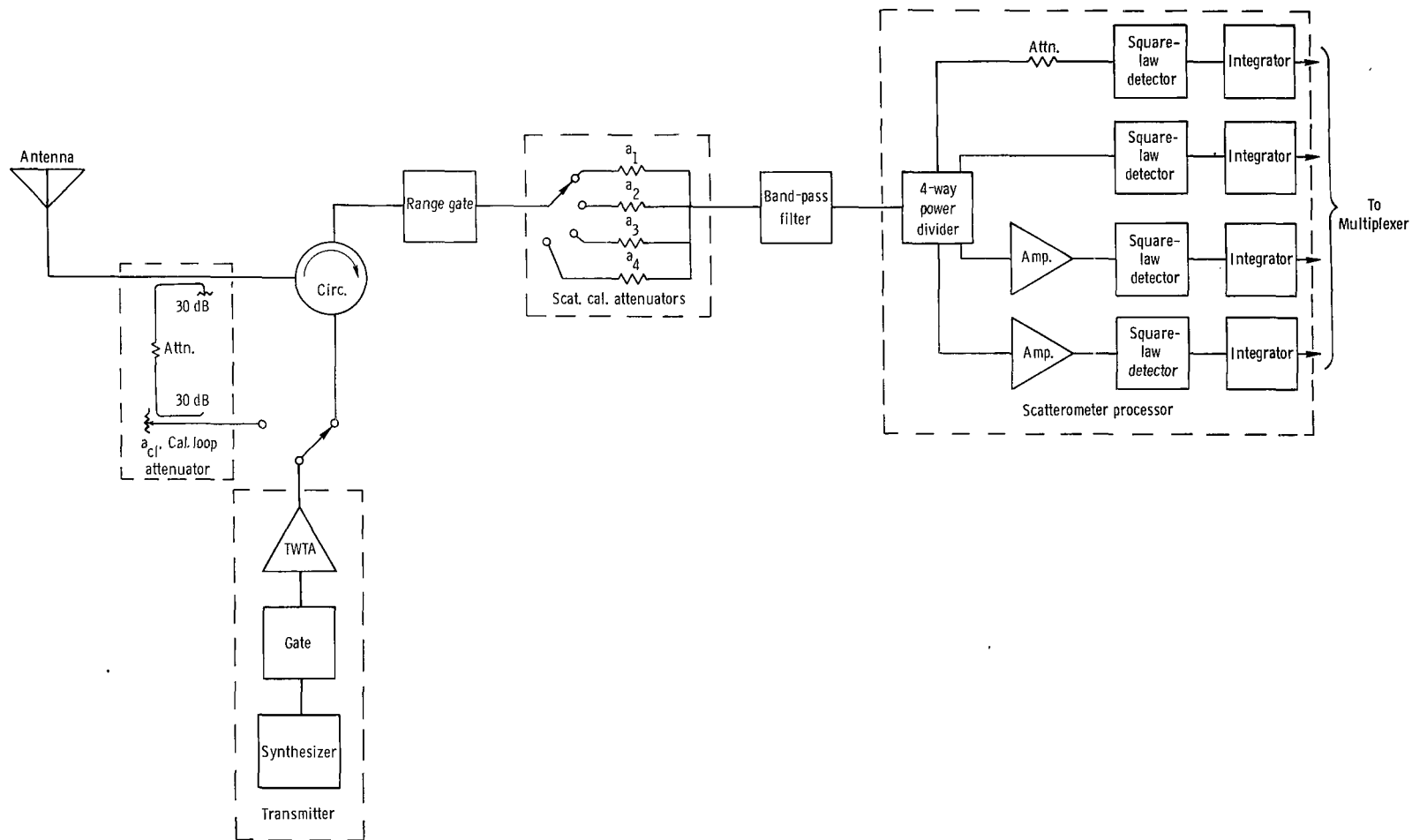
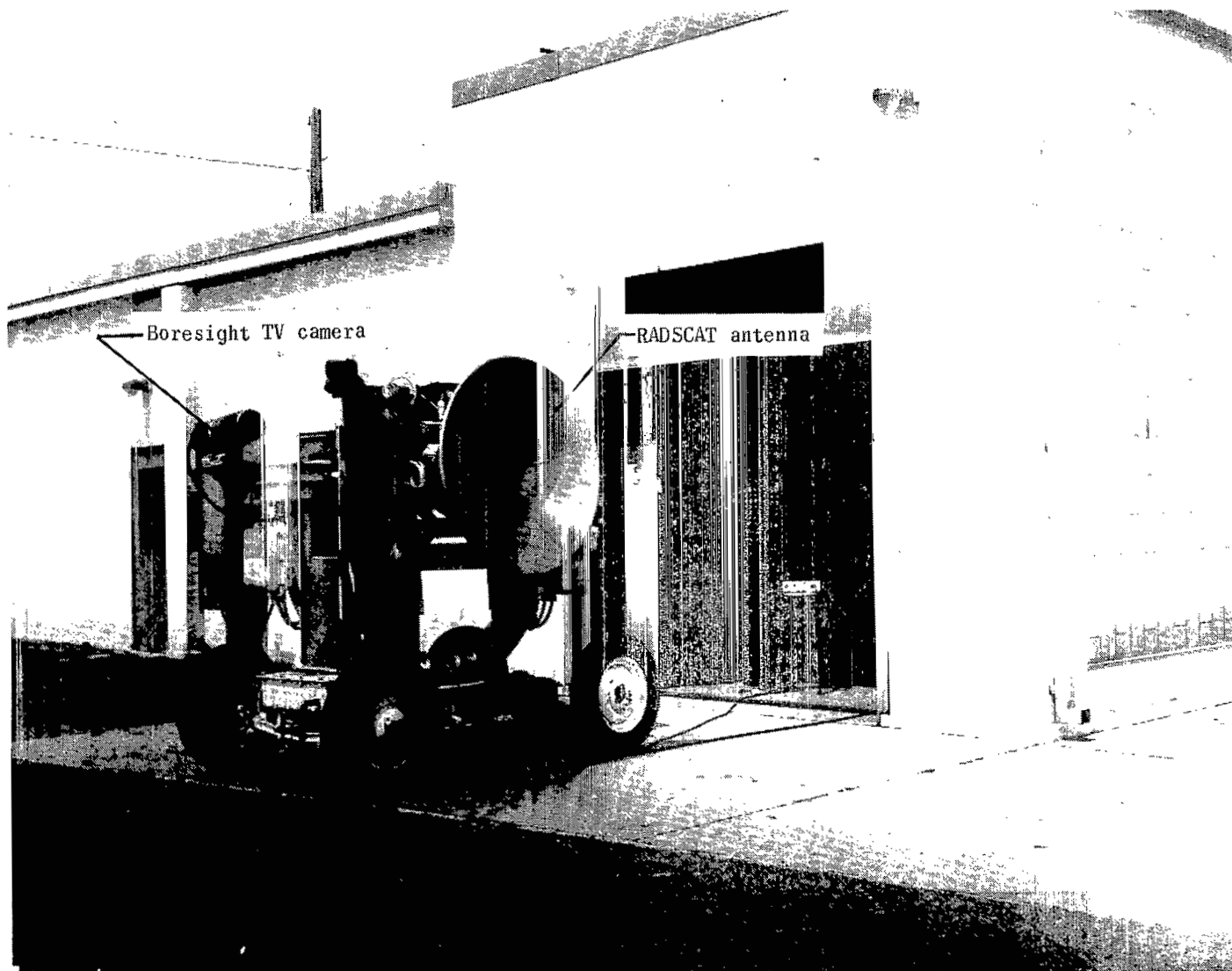


Figure 1.- Simplified block diagram of RADSCAT scatterometer.



L-72-78.1

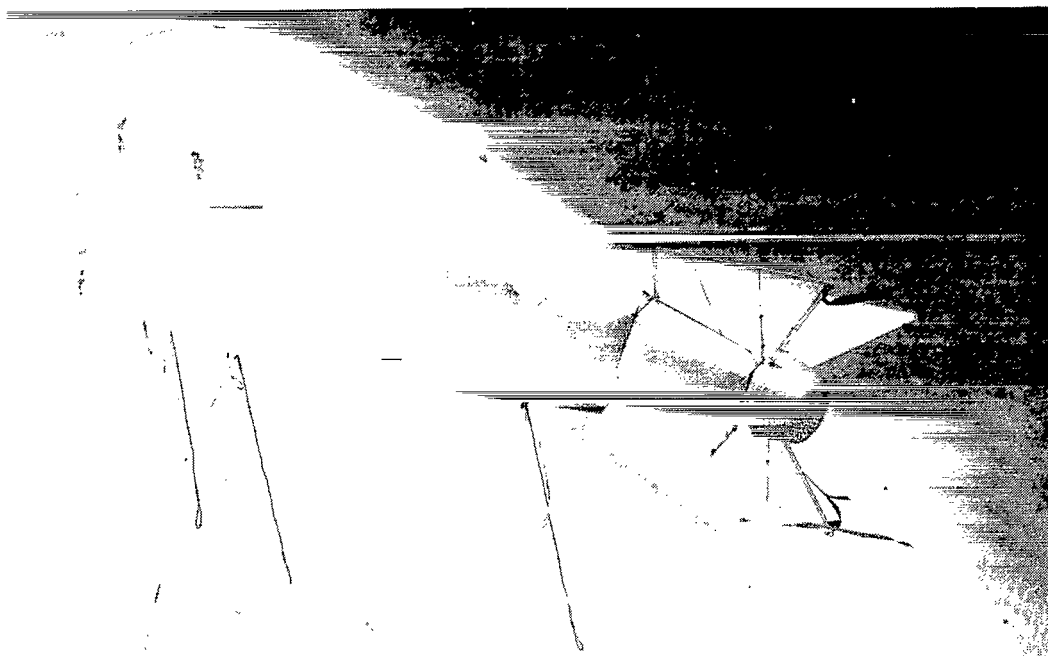
Figure 2.- RADSCAT installed on gimbaled mount for sphere calibration.

5
2
0
5



WI-73-510

Figure 3.-Sphere suspended from weather balloon.



(a) Kytoon, tethering lines, and harness. L-72-81



(b) Spheres and support netting. L-76-223

Figure 4.- Kytoon apparatus used for sphere calibrations.

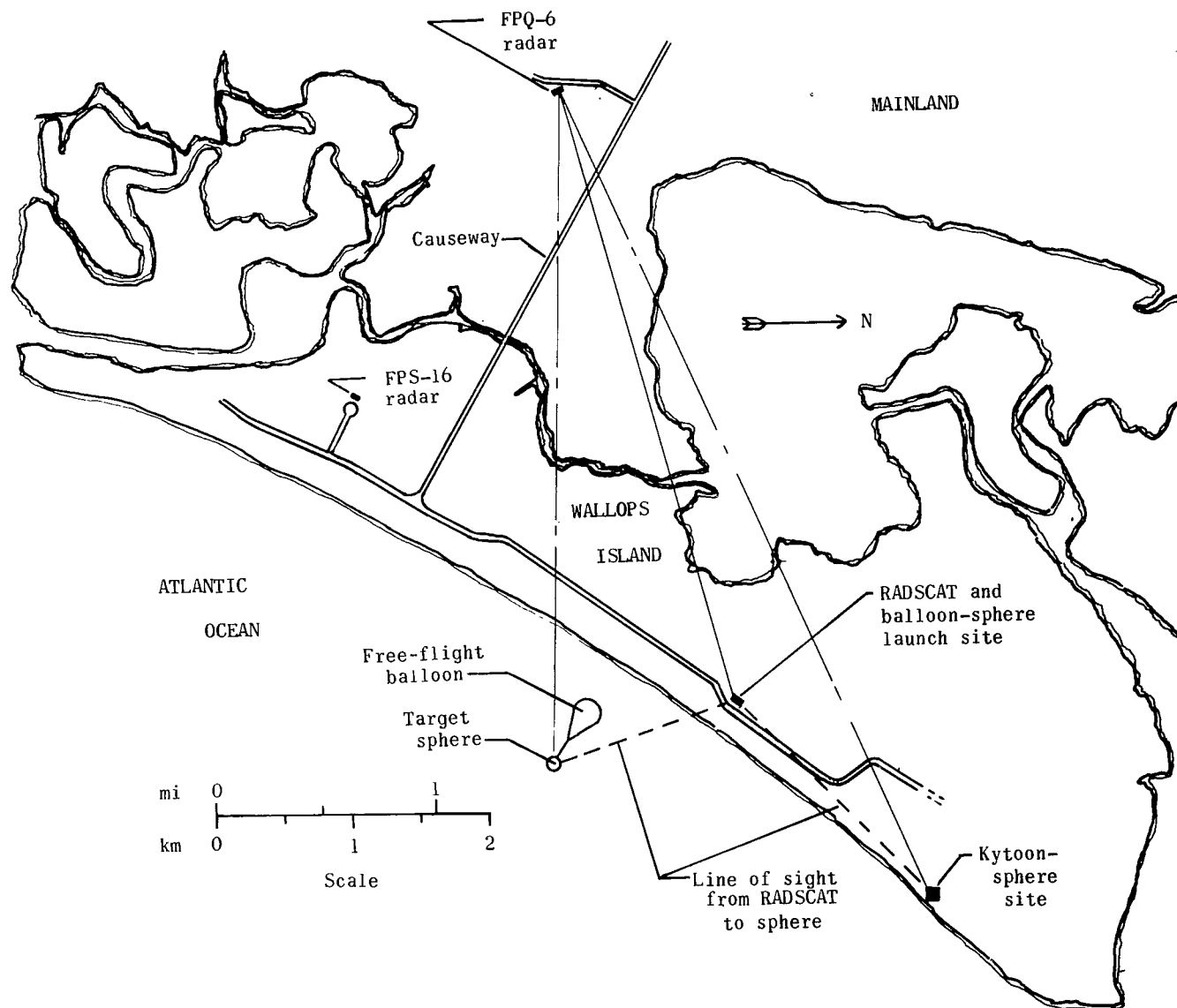


Figure 5.- Geometry for ground-based sphere tests at Wallops Flight Center.

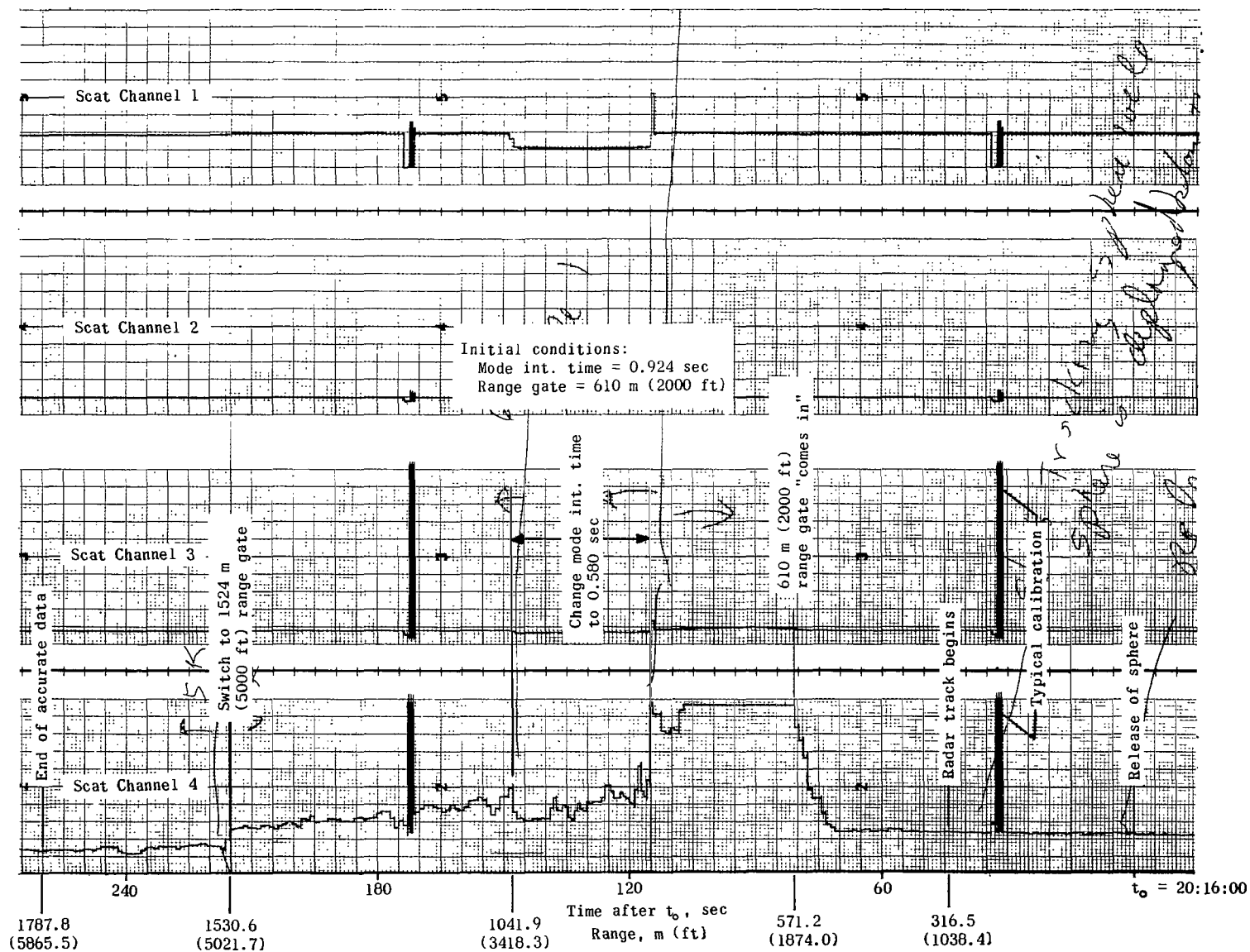


Figure 6.- Pen record for small-sphere test at 13.9 GHz.

Figure 7.- Pen record for large-sphere test at 13.9 GHz.

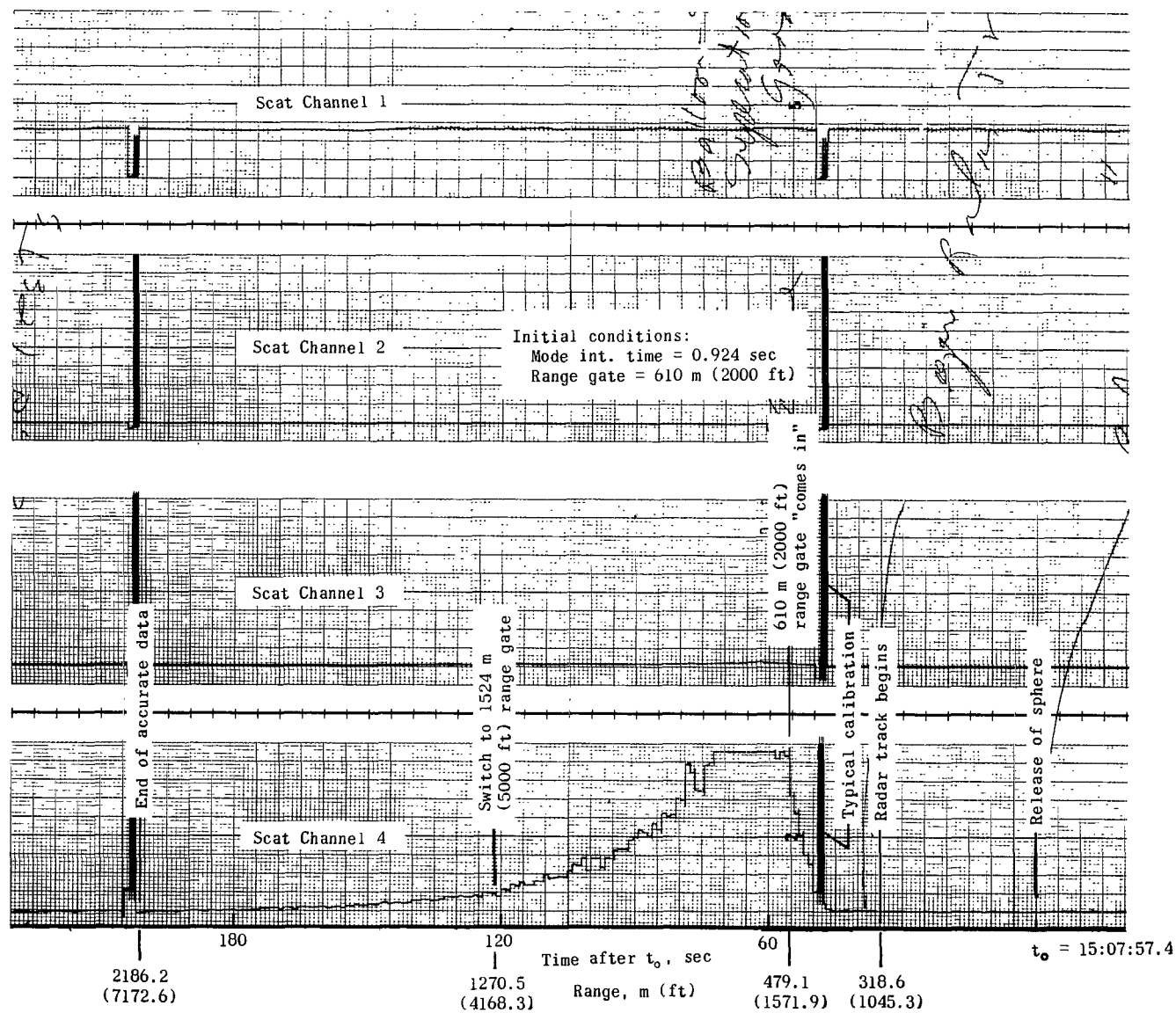


Figure 8.- Pen record for small-sphere test at 9.3 GHz.

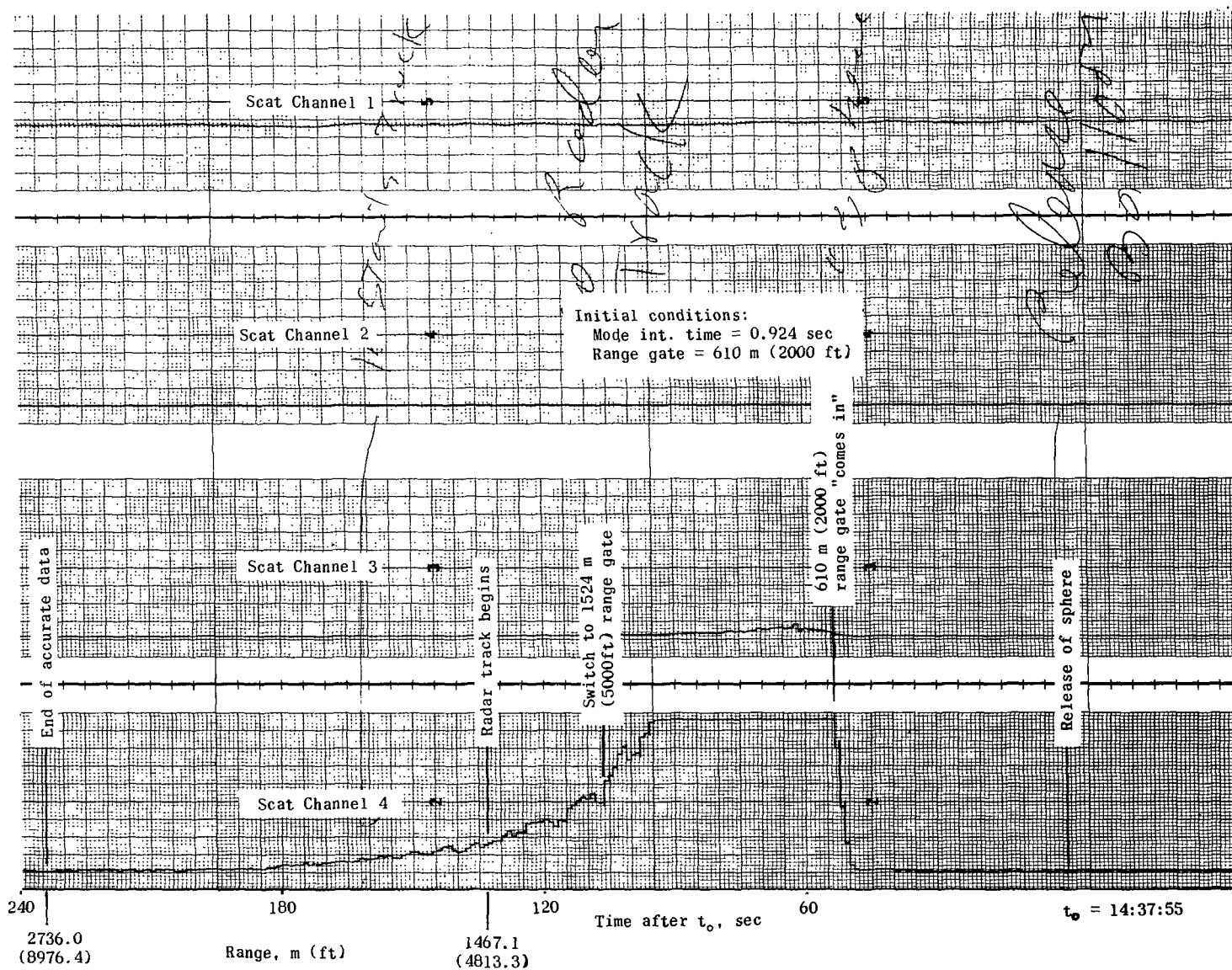


Figure 9.- Pen record for large-sphere test at 9.3 GHz.

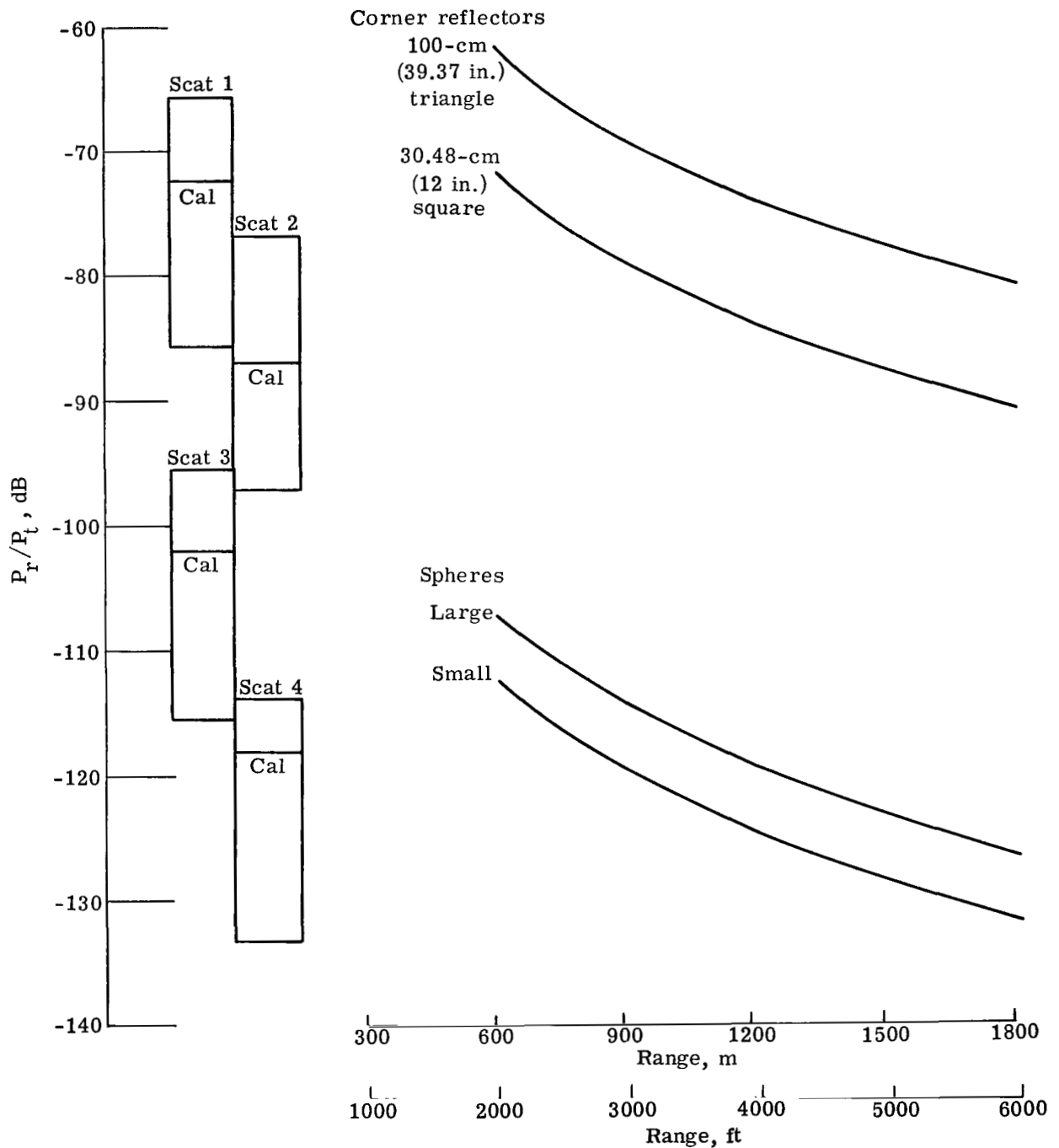


Figure 10.- RADSCAT theoretical target values for 13.9 GHz relative to RADSCAT dynamic range. RADSCAT dynamic range assumes average antenna gain is 38.22 dB and mode integration time is 0.924 sec. $P_{noise}/P_t = -150$ dBm.

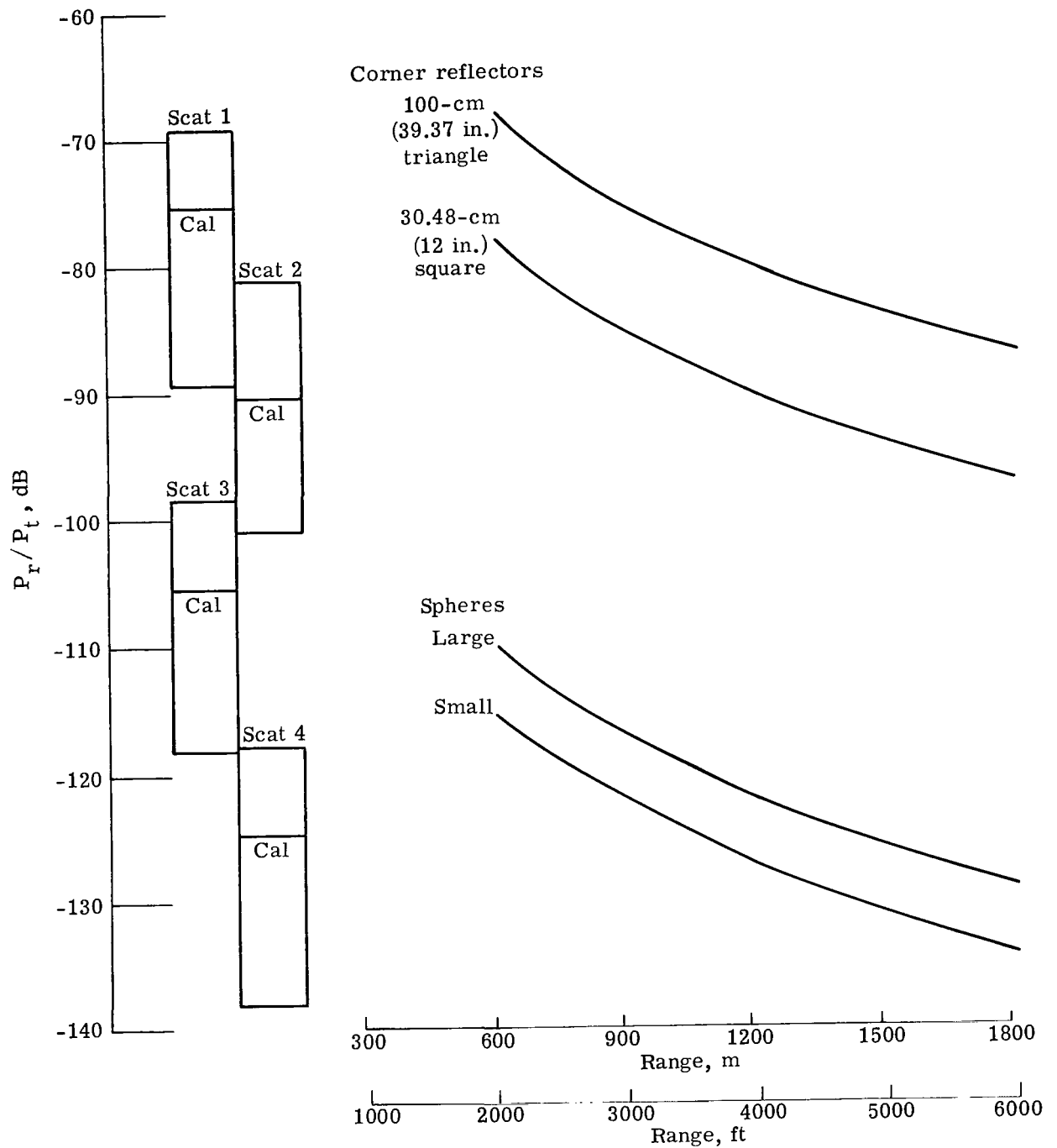


Figure 11.- RADSCAT theoretical target values for 9.3 GHz relative to RADSCAT dynamic range. RADSCAT dynamic range assumes average antenna gain is 29.99 dB and mode integration time is 0.924 sec. $P_{noise}/P_t = -152$ dBm.

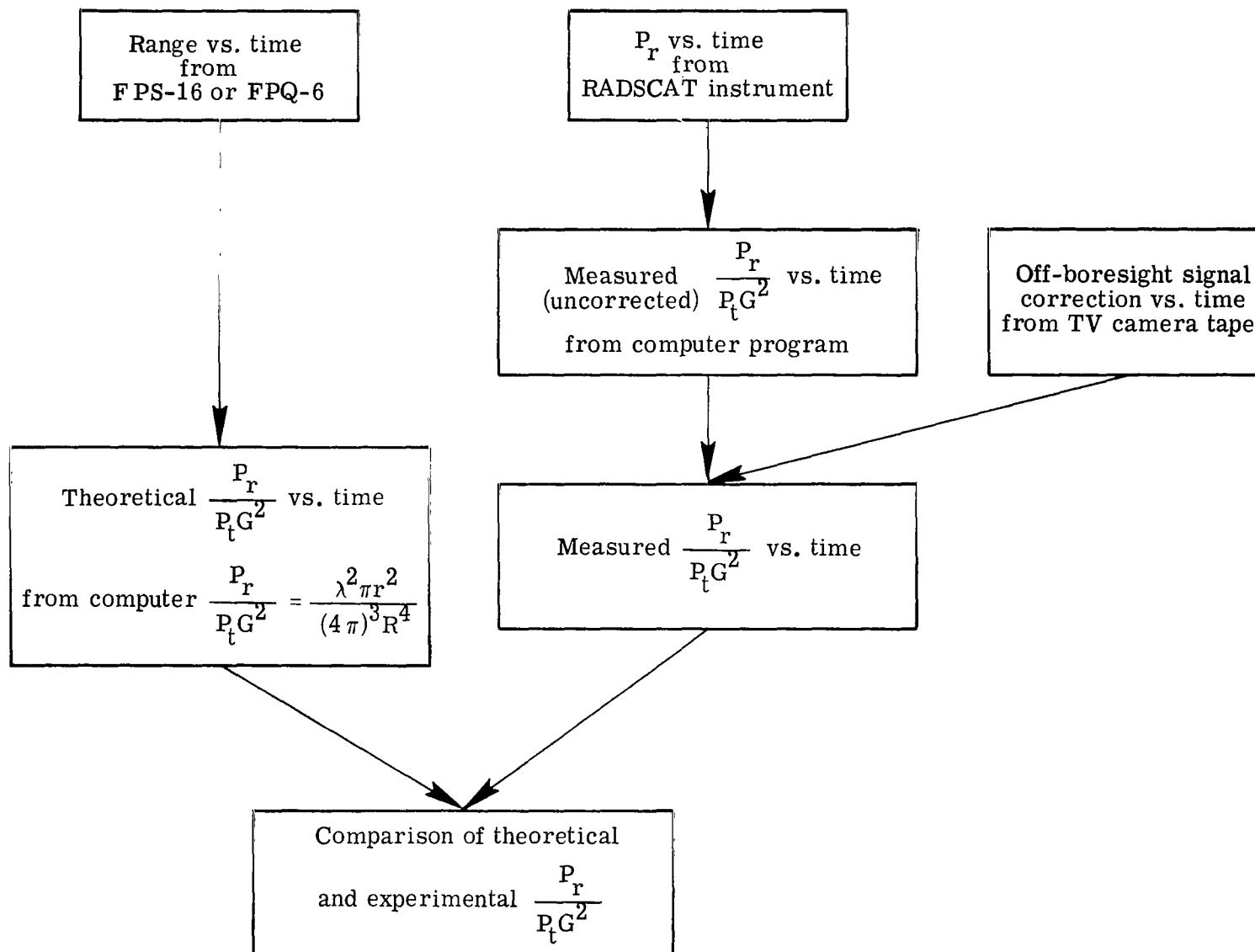


Figure 12.- Sphere data reduction procedure.

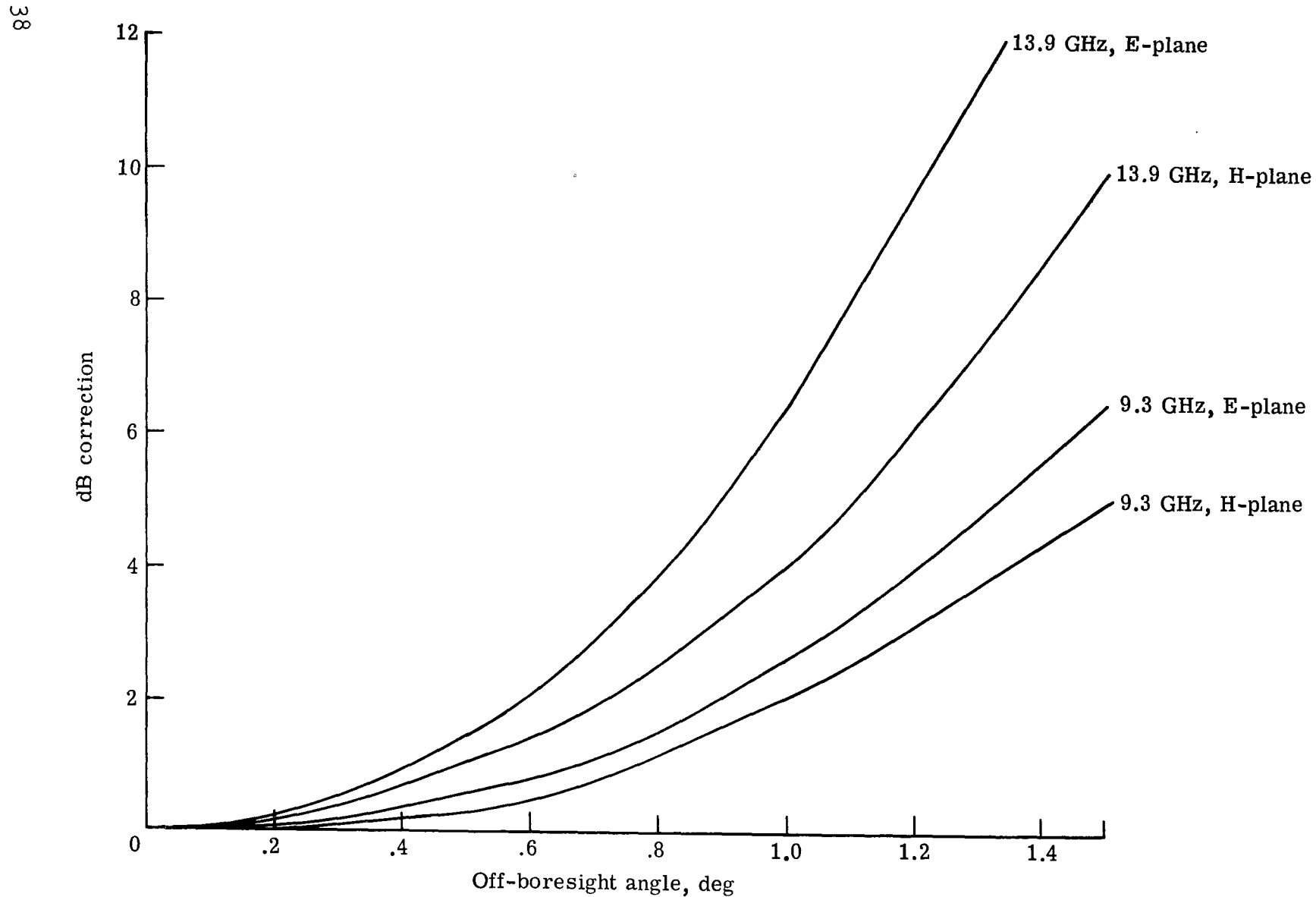


Figure 13.- Off-boresight signal level corrections derived from RADSCAT antenna patterns (dated 1-12-72 and 1-13-72).

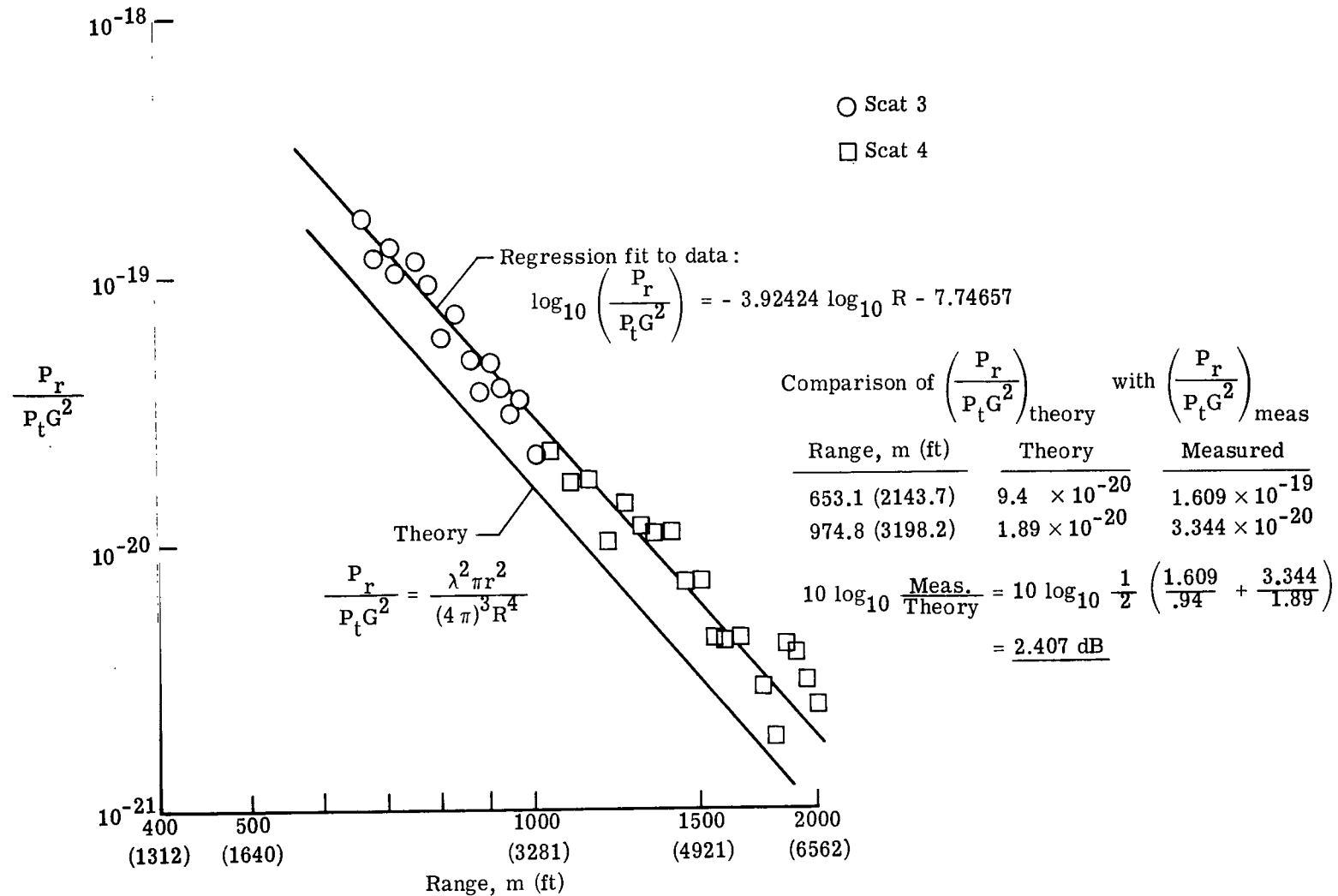


Figure 14.- RADSCAT small-sphere test results at 13.9 GHz.

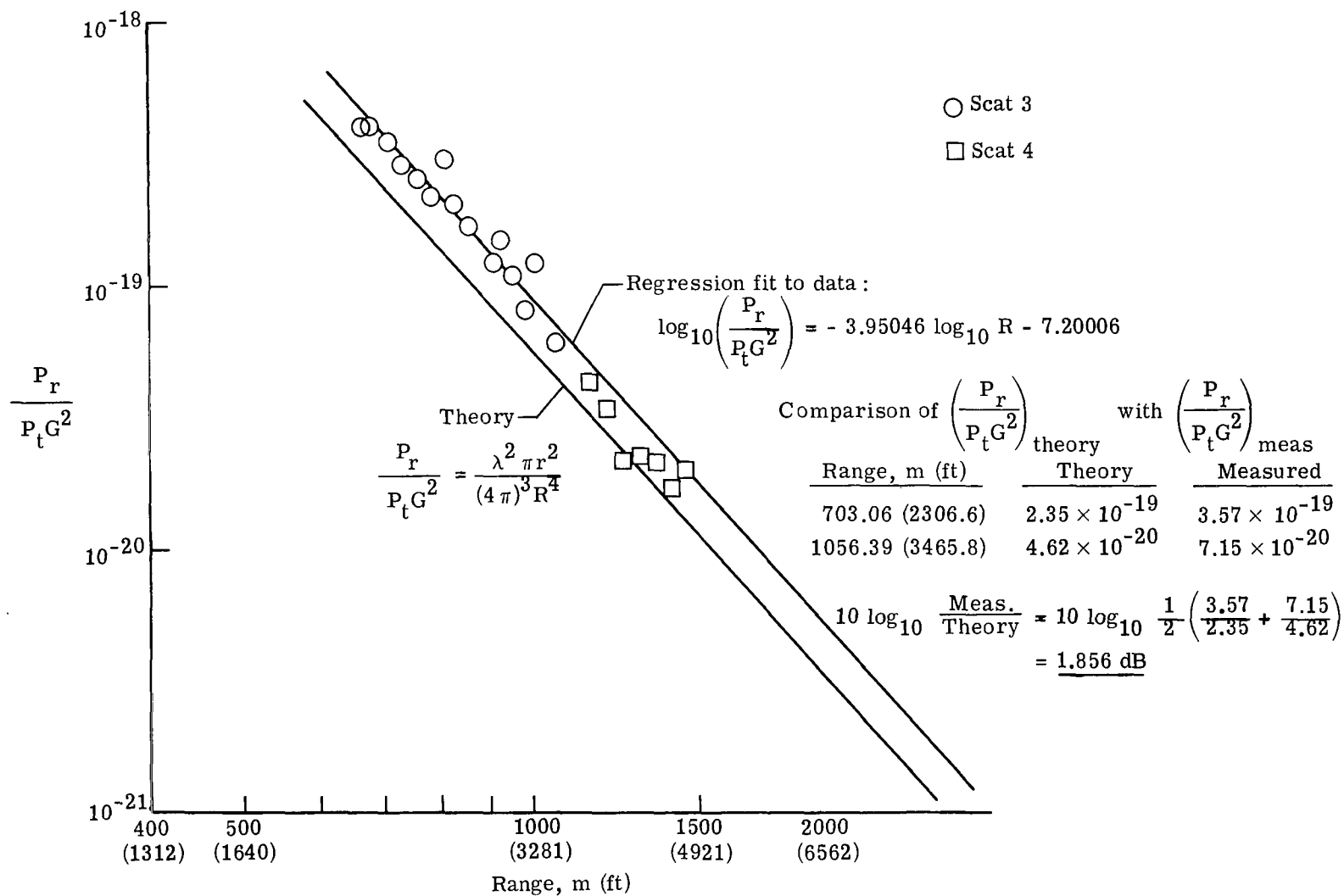


Figure 15.- RADSCAT large-sphere test results at 13.9 GHz.

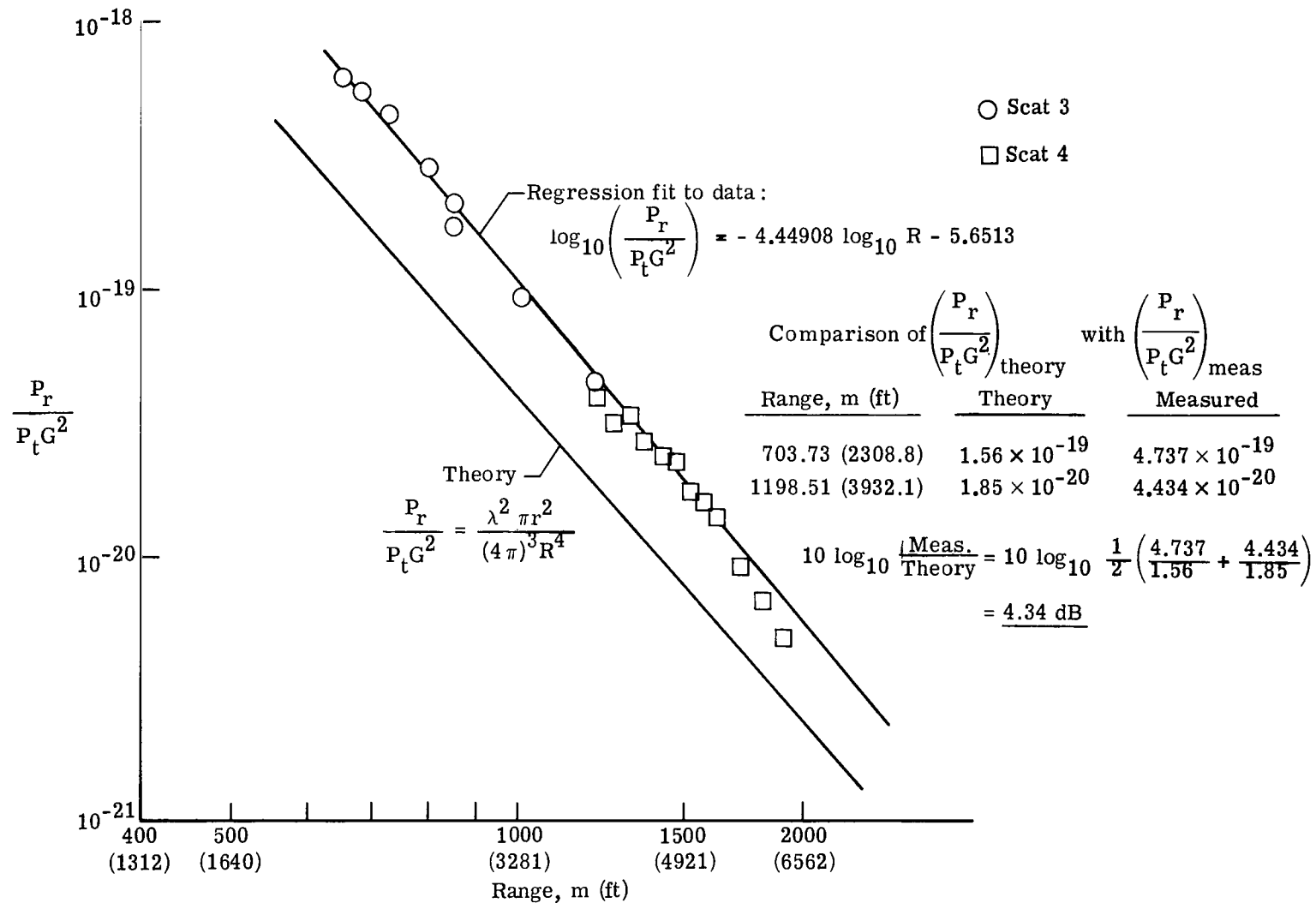


Figure 16.- RADSCAT small-sphere test results at 9.3 GHz.

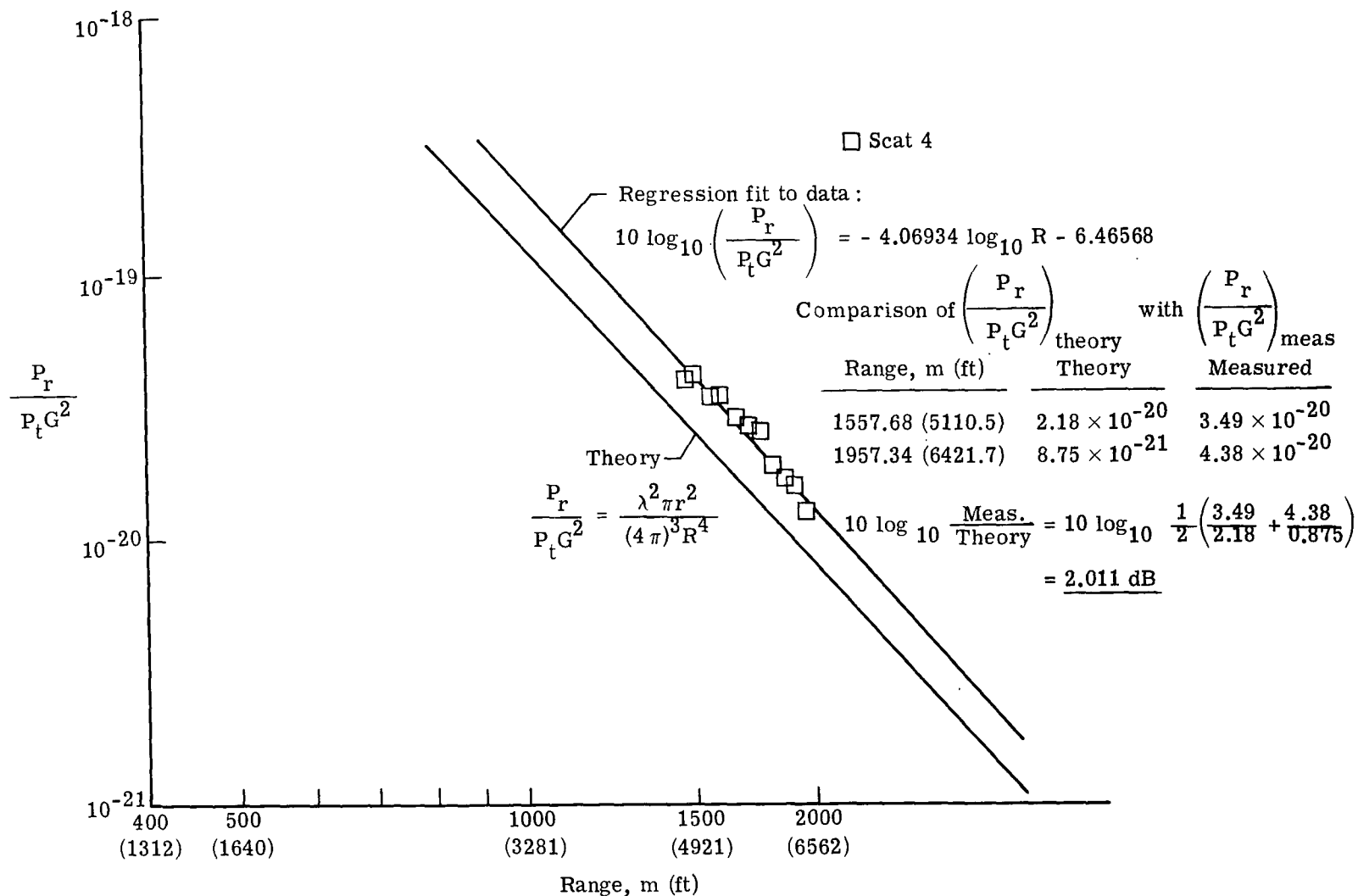


Figure 17.- RADSCAT large-sphere test results at 9.3 GHz.

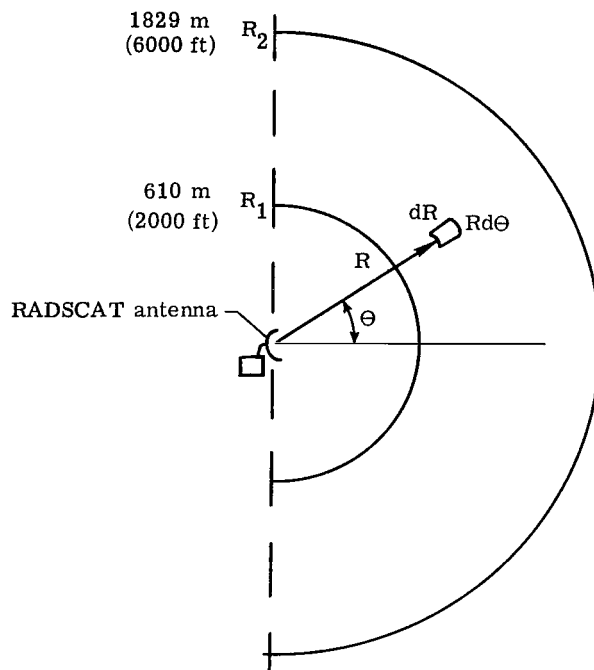


Figure 18.- Geometry of ground clutter error calculation.

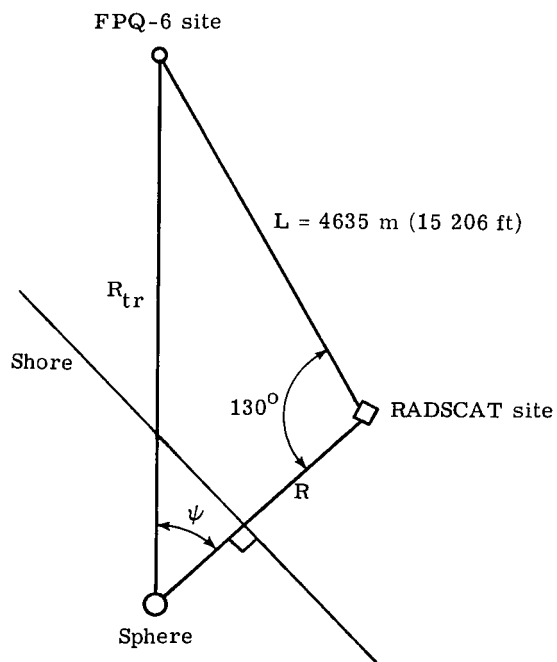


Figure 19.- Geometry of tracking radar range and angle error.



976 001 C1 U E 761210 S00903DS
DEPT OF THE AIR FORCE
AF WEAPONS LABORATORY
ATTN: TECHNICAL LIBRARY (SUL)
KIRTLAND AFB NM 87117

POSTMASTER: If Undeliverable (Section 158
Postal Manual) Do Not Return

"The aeronautical and space activities of the United States shall be conducted so as to contribute . . . to the expansion of human knowledge of phenomena in the atmosphere and space. The Administration shall provide for the widest practicable and appropriate dissemination of information concerning its activities and the results thereof."

—NATIONAL AERONAUTICS AND SPACE ACT OF 1958

NASA SCIENTIFIC AND TECHNICAL PUBLICATIONS

TECHNICAL REPORTS: Scientific and technical information considered important, complete, and a lasting contribution to existing knowledge.

TECHNICAL NOTES: Information less broad in scope but nevertheless of importance as a contribution to existing knowledge.

TECHNICAL MEMORANDUMS: Information receiving limited distribution because of preliminary data, security classification, or other reasons. Also includes conference proceedings with either limited or unlimited distribution.

CONTRACTOR REPORTS: Scientific and technical information generated under a NASA contract or grant and considered an important contribution to existing knowledge.

TECHNICAL TRANSLATIONS: Information published in a foreign language considered to merit NASA distribution in English.

SPECIAL PUBLICATIONS: Information derived from or of value to NASA activities. Publications include final reports of major projects, monographs, data compilations, handbooks, sourcebooks, and special bibliographies.

TECHNOLOGY UTILIZATION PUBLICATIONS: Information on technology used by NASA that may be of particular interest in commercial and other non-aerospace applications. Publications include Tech Briefs, Technology Utilization Reports and Technology Surveys.

Details on the availability of these publications may be obtained from:

SCIENTIFIC AND TECHNICAL INFORMATION OFFICE

NATIONAL AERONAUTICS AND SPACE ADMINISTRATION

Washington, D.C. 20546